Engineering Materials

Naveen Kumar
Virat Khanna
Nupur Aggarwal
Shalini Tripathi *Editors*

Rare Earth-Doped Metal Oxide Nanostructures

For Energy Harvesting and Environmental Sensing

Springer

Editors
Naveen Kumar
Department of Physics
Galgotias University
Greater Noida, Uttar Pradesh, India

Nupur Aggarwal
Department of Physics
Chandigarh University
Mohali, Punjab, India

Virat Khanna
University Centre for Research
and Development (UCRD)
Chandigarh University
Mohali, Punjab, India

Shalini Tripathi
Pacific Northwest National Laboratory
Energy and Environment Directorate
Richland, WA, USA

ISSN 1612-1317 ISSN 1868-1212 (electronic)
Engineering Materials
ISBN 978-981-95-6191-9 ISBN 978-981-95-6192-6 (eBook)
https://doi.org/10.1007/978-981-95-6192-6

Contents

Enhanced Adsorption and Degradation of Synthetic Dyes Using Rare Earth Metal-Doped Biodegradable Polymers

Amanpreet Kaur, Ayasha Negi, Shubhangee Agarwal, Man Vir Singh, Jitendra Pal Singh, and Neha Bhatt

Abstract The adverse environmental effects and health burdens associated with dye discharge have necessitated the adoption of photocatalytic degradation as an effective method for addressing water contamination. Recent studies in photocatalysis indicate that nanocomposites incorporating rare earth metals are essential for improving the degradation of dyes in sewage water treatment. This paper reviews the significance of degradation of dyes in the presence of light, highlighting its environmental benefits, sustainable characteristics, and versatility in a wide range of fields. The doping of rare earth metals in nanocomposites significantly enhances photocatalytic activity. This is achieved through an extended absorption range of the photocatalysts, which enhances charge segregation and ensures stable frameworks. REMs function as photosensitisers, creating sub-band-energy levels between the conduction band and valence band of nanocrystals (NCs). The REMs-doped NCs demonstrate enhanced efficiency in dye decomposition relative to conventional methods, attributable to alterations in band structures, improved charge separation, and increased surface area. Multiple characterization methods are utilized to examine the structural and morphological properties of REMs-doped NCs, providing significant insights into their photocatalytic activity. Optimization strategies such as morphology control, surface modification, co-doping, and heterojunction formation are crucial for enhancing the photocatalytic performance of REM-doped NCs in photocatalytic reactions. The roles of various rare earth metals, including cerium, praseodymium, neodymium, samarium, dysprosium, europium, gadolinium, erbium, lanthanum, terbium, and ytterbium, have been examined regarding their potential applications in environmental remediation

A. Kaur (✉) · A. Negi · S. Agarwal
Department of Chemistry, School of Sciences, IFTM University, Moradabad, Uttar Pradesh, India
e-mail: amanpreet2225@gmail.com

M. V. Singh
School of Applied and Life Sciences, UIT, Uttaranchal University, Dehradun, Uttarakhand, India

J. P. Singh
Department of Physics, School of Sciences, IFTM University, Uttar Pradesh, Moradabad, India

N. Bhatt
Department of Chemistry, Pt. L.M.S., Rishikesh Campus, SDS University, Tehri Garhwal, Uttarakhand, India

N. Kumar et al. (eds.), *Rare Earth-Doped Metal Oxide Nanostructures*, Engineering Materials, https://doi.org/10.1007/978-981-95-6192-6_4

via photocatalytic degradation of dyes. This review will provide a comprehensive analysis of current progress in the implementation of REMs-doped NCs for the enhancement of dye degradation, contributing to the development of more effective photocatalysts for water purification.

Keywords Photocatalysis · Dyes remediation · Rare earth metals · Environmental concerns

1 Introduction

Water is a limited and crucial resource for humanity, now confronting escalating worldwide issues, notably due to pollution. A significant environmental issue is wastewater tainted with dye as a result of industrial activities [1]. The textile, leather, paper, plastic, and printing industries saw significant expansion in the twentieth century, resulting in substantial quantities of synthetic dyes being released into aquatic ecosystems. Dyes and pigments are used worldwide, with an estimated variety exceeding 10,000 varieties and an annual production of approximately 0.7 million metric tonnes. Textile manufacture consumes significant quantities of water, around 200 L every kilogram of textile produced, with a normal mill using up to 1.6 million gallons daily.

The discharge of dye wastewater poses significant dangers to the environment. These pollutants obstruct sunlight penetration, disrupting the photosynthetic process in aquatic ecosystems, and are often composed of extremely poisonous heavy metals (e.g., lead, chromium) or aromatic compounds. The intricate aromatic ring structure renders the dye molecules very durable, preventing their degradation under standard treatment conditions (e.g., aerobic digestion, photolysis, heat treatment, and oxidation). Moreover, some dyes have mutagenic, carcinogenic, and cytotoxic properties, posing a risk to human health by potentially damaging the liver, kidneys, brain, reproductive system, and central nervous system.

Efforts to tackle these problems have been executed using several physicochemical and biological treatment methods. Among these technologies, adsorption has emerged as one of the most advantageous and cost-effective ways for dye removal, owing to its operational simplicity, efficacy, and economic viability [2]. Activated carbon is the standard adsorbent owing to its remarkable capacity (surface area) and adsorption properties. However, its elevated production costs and regeneration constraints hinder extensive use, particularly for low concentration or stubborn dyes that exhibit inadequate selectivity, such as dispersion and vat dyes [3].

Several attempts have been made in the recent past to formulate better alternative adsorbents that are both more efficient and economical. These include naturally occurring materials (e.g., clays, zeolites), biosorbents, agricultural by-products, industrial wastes, and their corresponding composites [4]. A significant amount of research has concentrated on modifying these materials to improve their surface characteristics, dye adsorption capabilities, and selectivity for different dye types.

Despite the abundance of novel adsorbent materials, there is a scarcity of thorough research examining dye adsorption from a macro viewpoint [5]. This study will categorize dyes according to their health and environmental risks, assess different dye removal methods, and analyze the adsorption isotherms pertinent to dye sorption [6]. It thoroughly encapsulates and synthesizes contemporary advances in alternative adsorbents, emphasizing their physicochemical properties, efficacy, and constraints across diverse environmental conditions [7]. The paper identifies fundamental challenges hindering the transition of these materials from laboratory-based discovery to industrial use. Ultimately, it delineates prospective avenues, including the development of multifunctional adsorbents, scalability constraints, and hybrid integration techniques, which are essential for the future progression of dye remediation technologies [8].

2 Rare Earth Metal-Doped Biodegradable Polymers for Dye Degradation

Nanomaterials have significantly revolutionized wastewater treatment technology, especially in the decolorization of dye effluents. Nanostructures, generally ranging from 1 to 100 nm, exhibit exceptional surface area-to-volume ratios, leading to enhanced physicochemical and catalytic activity relative to their bulk counterparts [9]. Metal oxides (MOs) are extensively researched nanomaterials that have shown efficacy in the degradation of organic contaminants in industrial effluent. These nanometal oxides were extensively used in remediation, optical, and mechanical systems [10]. Certain metal oxides, including ZnO, TiO_2, CeO_2, and La_2O_3, have shown significant efficacy in the photocatalytic destruction of dyes. Lanthanum oxide (La_2O_3), a rare-earth metal oxide, is distinguished by its substantial and broad band gap energy (4.3–5.8 eV) and its distinctive electrical structure. In contrast to other lanthanides, La^{3+} lacks 4f electrons and has an electronic configuration comparable to that of xenon [11]. This enhances its unique characteristics, making it suited for many applications. The many biological actions of rare-earth elements, such as lanthanum, which include anticoagulant, antiemetic, antibacterial, anticancer, and antioxidant properties, enhance their use in biomedical and pharmaceutical domains. Moreover, La_2O_3 has superior economic efficiency relative to other rare-earth oxides, including Y_2O_3 and Gd_2O_3 [12].

La_2O_3 nanoparticles have applications in hydrogen storage, superconductors, optoelectronic materials, laser crystals, LEDs, biosensors, high refractive index optical fibers, and catalysis. Furthermore, owing to its intrinsic characteristics, La_2O_3 rapidly interacts with ambient CO_2 to produce lanthanum carbonate, hence affecting its stability and crystalline qualities [13]. Nanostructured La_2O_3 has been synthesized via hydrothermal, sol–gel, thermal degradation, sonochemical, and co-precipitation methods. The co-precipitation technique is valued for its simplicity, affordability, and lack of need for specialized equipment.

The fabrication of La_2O_3 nanostructures significantly affects the physicochemical characteristics and the activity of the resultant catalysts. Molybdenum (Mo) may be used as a dopant to augment photocatalytic activity [14]. The inclusion of Mo promotes thermal stability, reduces the band gap, increases charge carrier concentration, and broadens the absorbing ability into the visible wavelengths of light. It further stabilizes the electronic band framework of metallic oxides semiconductors. Ikram et al. [15] synthesized undoped and Mo-doped La_2O_3 nanostructures (0.02, 0.04, and 0.06 wt % Mo) using the one-pot co-precipitation technique. The resulting materials were then evaluated for their antibacterial efficacy against *Staphylococcus aureus* and *Escherichia coli*, as well as their ability to degrade methylene blue (MB), a prevalent model dye [15]. The X-ray diffraction (XRD) examination indicated that La_2O_3 included both cubic and hexagonal structures. Doping does not influence the phase structure but markedly enhances the crystallinity. Density functional theory (DFT) and UV–Vis spectroscopy were employed to ascertain the optical properties of the products, confirming a reduction in the energy gap and the emergence of additional strong absorption bands upon Mo embedding [16]. High-resolution transmission electron microscopy (HR-TEM) revealed that La_2O_3 nanostructures were rod-shaped and exhibited increased density with increasing Mo content. Photocatalytic degradation experiments showed that molybdenum doping improved the degradation efficiency of methylene blue [17]. Increased Mo concentrations augmented antibacterial activity, as the inhibition zone measured 5.05 mm against *Staphylococcus aureus* and 5.45 mm against *Escherichia coli* at 6 wt% Mo doping [18]. In addition to these results, Singh et al. [19] assessed the photocatalytic efficacy of many oxides of metals, namely NiO, ZnO, CuO, CeO_2, SnO_2, and Mn_3O_4, concerning the degradation of methylene blue and methyl orange under UV–visible light. Each nanoparticle, at a concentration of 100 mg, has been suspended in 100 mL of dye mixture and subjected to irradiation for 2 h, with samples collected every 20 min [19]. ZnO has been identified as the most efficient catalyst, demonstrating exceptional removal efficacy for the two dyes.

These dynamics demonstrate the efficacy of nanostructured metal oxides, namely Mo-doped La_2O_3, as effective photocatalysts for environmental remediation. The substitution of Mo in La_2O_3 enhances optical and structural characteristics, significantly improves dye degradation and antibacterial activity, and presents promising opportunities for the development of multifunctional nanomaterials in sustainable wastewater treatment applications [20] (Table 4.1).

3 Metal-Incorporated Biopolymeric Nanomaterials

Metal-doped nanomaterials demonstrate improved efficacy in the photocatalytic destruction of azo dyes, principally owing to their customized pore structure, surface crystallography, and superior mechanical strength [31]. The core mechanism of photocatalytic degradation is a photo-induced electron transfer process, closely linked to redox processes. The introduction of metallic nanoparticles alters

Table 4.1 Strength and limitations of different dye degradation techniques

Methods	Strength	Limitations	References
Adsorption	The most advanced technology, effortless operation, and efficient removal of dyes from effluent	The adsorption efficiency is constrained by the environmental conditions and the structure of the adsorbent Secondary pollution is effortless to generate	[21]
Biochemical method	Specificity of biodegradation. Non-toxic impact on microorganisms	Processing speed is slow, and the ground occupies a significant area. Environmental conditions that are advantageous, including pH, temperature, and nutrition	[22]
Chemical oxidation	A prompt and comprehensive response. There is no secondary pollution	Excessive energy consumption Additional chemical reagents are necessary	[23]
Coagulation	Simple process and operation, minimal equipment cost, and high efficacy for hydrophobic dyes	The treatment procedure generates a substantial amount of sediment, which is challenging to dehydrate and inappropriate for the decolorization of hydrophilic pigments	[24]
Membrane separation	Selectivity to dyes, removal of a variety of dyes, and minimal space requirements	High initial, maintenance, and operational expenses The utilization of austere conditions (pressurization and effluent flow restrictions) Short service life and effortless obstruction	[25]
Photocatalysis	Thorough degradation of dyes and effective eradication of obstinate dye molecules High efficiency and energy conservation	It is challenging to distinguish between the active components and intermediate products Bad light transmittance with a poor effect on high concentration dye effluent	[26]
Nanofiltration	Absence of adsorbent depletion	The disposal of suspended effluent is a challenging process	[27]
Ozonation	Effective removal of pigmentation	Elevated electricity expenses necessitate	[28]
Fenton	Effective for both soluble and nonsoluble pigments	Creating aromatic compounds that may be detrimental to both human health and the environment	[29]
UV hydrogen peroxide photocatalysis	Pigments undergo degradation through the utilization of electrons	The cost is elevated by the substantial energy consumption of UV lamps	[30]

the semiconducting characteristics of the solution, facilitating interfacial charge transfer, reducing metal oxidation, and improving electron lifetime, which eventually enhances photocatalytic reactivity [32]. Surface plasmon resonance (SPR), often seen in nanoscale metallic nanoparticles, enhances localized electron density and optimizes charge carrier dynamics. Polymeric nanocomposites containing metallic nanoparticles work as self-stabilizing systems, enhancing dispersion and functional integration [33]. Metal-polymer hybrid materials, such as metal-infused resins, are widely used in industrial catalytic processes. Attaching metallic nanoparticles to polymeric matrices improves structural density and physicochemical stability while also providing unique functional characteristics compared to monomeric metal nanoparticles [34].

The size distribution of metal nanoparticles is typically heterogeneous; however, the introduction of a polymer matrix facilitates particle size homogeneity and enhances overall system stability. This is shown by the integration of bacterial cellulose fibers with gold nanoparticles (AuNPs). Gold nanoparticles (AuNPs), averaging 74.32 nm in size and generated from fresh fruiting bodies of *Flammulinavelutipes* (Enoki mushroom), effectively degrade roughly 75% of methylene blue dye after 4 h. The extensive substrate specificity of AuNPs facilitates the degradation of many organic dyes [35]. The f-orbital electrons of lanthanum (La) interact with different functional groups of biopolymers, resulting in the creation of coordination complexes with increased surface areas. The integration of La into biopolymeric matrices improves photocatalytic efficacy, especially in the destruction of organic contaminants like azo dyes [2]. A lanthanum-chitosan compound achieved 90% degradation of methylene blue in 40 min. This approach led to a substantial decrease in chemical oxygen demand (COD), roughly by a factor of eight, indicating efficient mineralization of the dye [36]. Figure 4.1 represents the Synthesis of Rare Earth Metal-Doped Biodegradable Polymers for photocatalytic dye degradation.

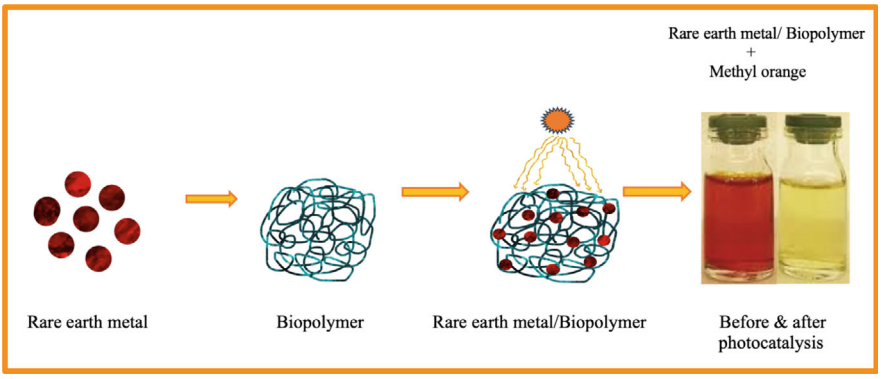

Fig. 4.1 Synthesis of rare earth metal-doped biodegradable polymers for photocatalytic dye degradation

4 Photo-Catalytic Characteristics of Rare Earth-Doped Metallic Oxides

Oxides of different metals are essential constituents in photocatalytic water splitting processes owing to their semiconducting characteristics. Cadmium sulfide (CdS), a metal sulfide, has been thoroughly studied for hydrogen (H_2) production; yet, its photocatalytic effectiveness is inadequate, mainly because of photocorrosion and rapid charge carrier reconstitution [37]. Like metal sulfides, several metal oxides have been investigated for photocatalytic uses. Titanium dioxide (TiO_2) and zinc oxide (ZnO) are prominently researched nanomaterials in this domain. However, their substantial band gaps (≈ 3.2 eV) considerably restrict their capacity to absorb visible light, leading to diminished quantum efficiency in photocatalytic processes [38]. To address these constraints, the integration of foreign dopants, especially rare earth elements, has surfaced as an effective technique to improve quantum yield and overall photo-degradation efficacy. Rare earth doping has shown the ability to enhance charge carrier isolation and inhibit the recombining of photo induced electron–hole pairs, thereby enhancing photocatalytic efficiency [39]. The mechanical justification for using rare earth elements as dopants is thoroughly detailed in the following section.

5 Rare Earth Metal Doped Metal Oxides

The distinct physicochemical characteristics of rare earth metal-doped metal oxides, such as their intense redox activity, excellent thermal stability, and customized electronic structures, have made them become cutting-edge functional materials. Rare earth elements like La, Ce, Eu, or Nd may be doped into metal oxides like TiO_2, ZnO, or CeO_2 to greatly increase their surface area, optical absorption, and catalytic activity. Improved charge carrier mobility and separation are made possible by these changes, which are essential for uses in environmental cleanup, gas sensing, and photocatalysis. By introducing localized energy states inside the bandgap, rare earth ions improve reaction kinetics in surface-driven processes and allow for more efficient use of visible light.

5.1 Gd-Doped Metal Oxides Nanoparticles

Multiple investigations have shown the efficacy of rare earth metal doping, namely gadolinium (Gd), in augmenting the photocatalytic efficiency of semiconductor nanomaterials used for splitting of water and breakdown of dyes. Mahalakshmi et al. indicated that the introduction of Gd ions into TiO_2 enhances its band gap energy and promotes superior charge carrier separation, thereby diminishing electron–hole pair recombination [40]. Moreover, Gd doping leads to a decrease in TiO_2 nanoparticle

dimensions, hence augmenting surface area and catalytic efficacy. The introduction of 0.03 wt% Gd doping in TiO_2 markedly enhanced its degrading efficiency, owing to the half-filled 4f orbital of Gd^{3+} ions, which efficiently capture electrons and facilitate interfacial charge transfer at the solid–liquid interface [41]. Although ZnO is acknowledged as a promising semiconductor for photocatalysis, its actual effectiveness is often limited by the fast recombining of photogenerated electron–hole pairs. Kalam et al., investigated Gd-doped ZnO nanoparticles, discovering improved charge separation, diminished particle size, and augmented surface area. Their research also emphasized the impact of calcination duration on photocatalytic efficacy. ZnO doped with Gd and calcined at 500 °C for 7 h demonstrated excellent photocatalytic activity; however, extended calcination (9 h) resulted in particle aggregation, increased crystallite size, and decreased surface area, thereby reducing activity [42]. Photoluminescence (PL) spectroscopy further validated that Gd doping causes a shift in emission spectra, signifying reduced electron–hole recombination. Selvaraj et al. produced Gd-doped ZnO nanorods by a sonochemical process and assessed their photocatalytic effectiveness for the breakdown of methylene blue (MB) under ultraviolet illumination. No deterioration was found after 300 min in the absence of a catalyst. Nonetheless, the use of Gd-doped ZnO markedly enhanced photocatalytic activity. A doping concentration of 3 wt% Gd resulted in a 92.76% degradation of MB after 300 min [43]. The research revealed that alkaline circumstances (pH 10) augmented photocatalytic activity, presumably owing to heightened production of hydroxyl radicals that promote oxidation. At pH 10, total (100%) degradation of MB dye was accomplished within 270 min using 3% Gd-doped ZnO. These data indicate that photocatalytic effectiveness is significantly influenced by the pH of the solution. Zhang et al. investigated the size-dependent photocatalytic properties of Gd-doped bismuth ferrite ($BiFeO_3$, BFO), a substance with an appropriate band gap of around 2.2 eV [44]. While pure BFO exhibits photocatalytic activity, it is hindered by elevated recombination rates of charge carriers. Gd doping led to a progressive diminution in particle size and an enhancement in outer area. Studies on the deterioration of Rhodamine B (RhB) indicated that pure BFO destroyed just 22.3% of RhB under visible light after 270 min, whereas Gd-doped BFO (at 1%, 3%, and 5%) had degradation rates of 34.2%, 56.8%, and 42.1%, respectively [45]. The 3% Gd-doped BFO had the greatest photocatalytic efficacy. SEM investigations revealed that increased Gd concentration resulted in reduced particle size while simultaneously enhancing agglomeration, which may impede photocatalytic activity by restricting access to active sites. Therefore, determining an ideal dopant concentration is crucial for enhancing photocatalytic performance [46].

In a separate investigation, Al-Hamdi et al. produced Gd-doped SnO_2 nanoparticles and assessed their efficacy in degrading phenol under sunshine and exposure to visible light. The photo catalysis efficacy of Gd-doped SnO_2 was evaluated against other rare earth-doped TiO_2 systems, namely those doped with Ce, Nd, and La. Among them, Gd-doped TiO_2 demonstrated exceptional performance, underscoring Gd's efficacy as a powerful dopant for augmenting photocatalytic processes [47].

5.2 Ce-Doped Metal Oxides Nanoparticles

Titanium dioxide (TiO_2) is acknowledged as a proficient photocatalyst; however, its extensive band gap constrains its photocatalytic efficacy during visible light exposure. Shi et al. found that the incorporation of cerium (Ce) into TiO_2 markedly improves its photocatalytic efficacy [48]. Cerium, owing to its partly occupied 4f and 4d orbitals, serves as an effective catalytic center and promotes photocatalytic interactions with organic molecules. The existence of empty orbitals in Ce facilitates efficient interaction with diverse functional groups. The researchers generated Ce-doped TiO_2 nanoparticles by integrating varying amounts of Ce, thereafter subjecting them to calcination at 500 °C [49]. X-ray diffraction (XRD) research illustrated that an increase in Ce levels induces to larger and less strong diffraction peaks of TiO_2, indicating a decrease in crystallite size. The diminishment of nanoparticle size results in an increased specific surface area, consequently augmenting redox activity and raising charge transfer capacity of photo-generated electron–hole pairs, eventually elevating photocatalytic performance [50].

The UV–Visible wavelengths of absorption of Ce-doped TiO_2 displayed a redshift, broadening the absorption edge into the visible light spectrum (400–600 nm), indicating enhanced photocatalytic activity under the visible light [51]. This differs from clean TiO_2, which mostly absorbs in the ultraviolet spectrum. Mora et al. examined the photocatalytic characteristics of cerium-doped ZnO, which intrinsically has a broad band gap of 3.37 eV [52]. Although ZnO is a promising photocatalyst, its efficacy is limited by the rapid charge carrier recombination. Rare-earth elements doping with elements like Ce are recognized for generating photo-induced charge transport mechanisms and inhibiting recombination of electron–hole. Moreover, rare-earth doping may decrease the gap between the bands, so promoting the excitation of electrons from the valence band to the conduction band [53]. Mora et al. produced Ce-doped ZnO nanoparticles with varying Ce amount in solution (0.5, 1.39, 2.55, 3.28, 3.71, and 4.14%). Studies on photocatalytic degradation indicated that an increase in Ce content improved photocatalytic activity, reaching an optimum concentration of 3.28%. Photocatalytic effectiveness decreased above this concentration under UV–Visible irradiation [52]. At a Ce doping level of 3.28%, the degradation of Direct Red 23 (DR-23) was completed in 70 min, while other concentrations required 110 min, demonstrating that this doping level provides the most effective photocatalytic performance. Meshram et al. produced cerium-doped ZnO nanoparticles for the breakdown of MB. Their results demonstrated that Ce doping lowers the gap between the bands and reduces particle size, both of which enhance photocatalytic efficiency [54]. The degradation efficiency improved from 49% with undoped ZnO to 69% with 3% Ce-doped ZnO in 30 min, underscoring the boost in degradation kinetics [55]. Liu et al. produced cerium-doped titanium dioxide nanosheets by a one-pot hydrothermal technique and evaluated their photocatalytic efficacy via the deterioration of RhB under UV–Visible irradiation. Fluorescence spectroscopy revealed that augmenting Ce concentration to 0.5% decreased fluorescence intensity, signifying inhibited electron–hole recombination and improved charge separation [29]. Nonetheless, a further

rise in Ce concentration resulted in elevated fluorescence intensity, indicating heightened recombination rates and diminished photocatalytic efficiency [56]. The sample with least doping, i.e., 2% Ce doping had the lowest photocatalytic degradation efficiency under UV–Visible light, highlighting the need of adjusting dopant amount [57].

5.3 Sm-Doped Metal Oxides Nanoparticles

Milanova et al. indicated that doping titanium dioxide (TiO_2) with samarium (Sm), produced by an ultrasonic-assisted sol–gel technique utilizing acetic acid as both solvent and catalyst, results in improved photocatalytic efficacy [58]. Their research demonstrated that the photocatalytic efficacy of TiO_2 fluctuates markedly with the concentration of the Sm dopant. A rise in Sm percentage corresponded with an enlarged surface area of the resultant nanocrystals. The photocatalytic activity was assessed using Alizarin Red S (ARS) dye as a model contaminant. TiO_2 doped with 1% Sm had the maximum activity, with around 93% dye degradation [59]. This improvement is due to reduced particle size, augmented BET surface area, and efficient inhibition of electron–hole recombination. Arasi et al. produced Sm-doped TiO_2 by a hydrothermal technique and examined its photocatalytic efficacy in degrading Rhodamine B (RhB). The studies, using 60 mg of catalyst in 60 mL of RhB solution, demonstrated a significant increase in degradation efficiency from 88% (pure TiO_2) to 95.76% after Sm doping. These results further validate that the introduction of Sm into TiO_2 elevates photocatalytic activity by improving quantum efficiency [60].

Benammaret al. investigated Sm-doped into TiO_2 nanoparticles for the photocatalytic breakdown of methanol. The presence of Sm was seen to augment photocatalytic efficiency, possibly attributable to the capability of Sm^{3+} ions to capture photogenerated charge carriers, hence facilitating electron/hole transfer to the retain oxygen molecules on the outer layer [61]. The study employing Diffuse Reflectance Spectroscopy (DRS) revealed a shift in the wavelength in the absorption spectra subsequent to Sm inclusion, indicating that electrons were effectively trapped in the conduction band by adsorbed oxygen, while photogenerated holes were efficiently captured by hydroxyl groups or water molecules. This mechanism facilitates the synthesis of hydroxyl radicals, which enhances the level of photocatalytic activity [62].

Faraz et al. sought to examine the impact of Sm doping levels on the photocatalytic capabilities of ZnO nanoparticles by using a gel-combustion process to produce Sm-doped ZnO nanoparticles. This work demonstrated that the inclusion of Sm generates surface imperfections advantageous for photocatalysis and causes a redshift in the absorption edge, enabling Sm to absorb visible light. Samarium-doped ZnO nanoparticles with 1, 3, and 5% Sm concentrations showed band gap energies of 3.25, 3.10, and 3.05 eV each, therefore demonstrating that the gap between the bands decreases with an increase in Sm concentration [63]. The photocatalytic activity was

assessed by degrading Malachite Green (MG) dye under visible light exposure. The 3% Sm-doped ZnO had the greatest photocatalytic efficiency. Exceeding this ideal concentration of Sm led to a reduction in photocatalytic activity, presumably owing to enhanced electron–hole recombination and a drop in defect density [64]. The results indicate that low levels of Sm^{3+} effectively capture photogenerated electrons and inhibit recombination, thus prolonging charge carrier lifetimes. UV–Vis absorption spectra reveal that 3% Sm doping leads to an absorption onset at approximately 400 nm, confirming enhanced visible light responsiveness and a diminished energy of band gaps relative to undoped ZnO [65]. In summary, samarium doping in TiO_2 and ZnO significantly improves photocatalytic activity by augmenting surface area, inhibiting charge recombination, and broadening light absorption into the visible spectrum. Nevertheless, the concentration of Sm must be carefully controlled, since excessive doping may result in detrimental effects on photocatalytic effectiveness [66].

5.4 Dy-Doped Metal Oxides

Farooq et al. examined the augmentation of photocatalytic activity in ZnO nanoparticles by doping with dysprosium ions (Dy^{3+}). The Dy-doped ZnO nanoparticles were produced by a sonochemical technique, and their photocatalytic efficacy was assessed utilizing an azo dye as a model contaminant. Scanning Electron Microscopy (SEM) study demonstrated that undoped ZnO nanoparticles had irregular shape and considerable aggregation, resulting in enlarged grain size and decreased surface area both adverse to photocatalytic effectiveness [67]. Doping ZnO with Dy^{3+} ions markedly reduced nanoparticle aggregation and modified the grain size, leading to a considerable increase in surface area. This decrease in aggregation not only enhanced the dispersion of nanoparticles but also reduced photo-generated charge recombination and photo-corrosion, consequently increasing the availability of photoactive sites and improving photocatalytic activity [68]. Phuruangrat et al. generated gadolinium-doped molybdenum trioxide (Gd-doped MoO_3) nanobelts and dysprosium-doped zinc tungstate (Dy-doped $ZnWO_4$) nanorods by a hydrothermal technique. The degradation of methylene blue (MB) dye when exposed to visible light was used to measure the photocatalytic effectiveness of the produced materials. Pure MoO_3 nanobelts demonstrated restricted photocatalytic efficacy, achieving just 77.34% degradation of MB in 30 min [69]. Upon doping with 3% Dy^{3+}, the degradation efficiency significantly enhanced to 97.76%, underscoring the essential function of Dy^{3+} in improving light absorption and charge carrier separation. Dy-doped $ZnWO_4$ nanorods, at a 3% doping concentration, achieved 97.46% destruction of MB after 30 min under visible light, underscoring their exceptional efficiency.

These studies collectively illustrate that rare-earth doping, specifically Dy^{3+} and Gd^{3+}, into diverse semiconductor matrices (ZnO, MoO_3, $ZnWO_4$) significantly enhances photocatalytic performance by augmenting surface area, minimizing agglomeration, inhibiting electron–hole recombination, and broadening light absorption into the visible spectrum [70].

5.5 Er-Doped Metal Oxides

Ahmad et al. produced ZnO nanoparticles doped by erbium (Er^3) by utilizing homogeneous precipitation approaches to increase the photocatalytic efficiency of undoped ZnO. Scanning Electron Microscopy (SEM) demonstrated a consistent morphology characterized by a smaller particle size distribution and the absence of apparent aggregation in the doped samples [71]. The crystal structure remained invariant after Er^{3+} doping. UV–Vis absorption analyses indicated a little wavelength shift in the absorption edge, implying enhanced visible light absorption. The photocatalytic process was assessed by the deterioration of methylene blue (MB) dye. Pure ZnO attained a degradation efficiency of 69.28% in 1 h, but Er-doped ZnO demonstrated improved efficiencies of 86.3%, 97.7%, and 91.3% for doping concentrations of 2.1%, 4.8%, and 6.3%, respectively [72]. A doping concentration of 4.8% yielded the maximum photocatalytic activity; any further increase resulted in a decrease, perhaps owing to the formation of recombination centers generated by excess dopants.

Bhatia et al. used a straightforward combustion technique to produce Er-doped ZnO nanoparticles at different concentrations 2.0, 2.5, 3.0, and 3.5 atomic weight percent, referred to as EZ1 through EZ4. X-ray diffraction (XRD) verified the presence of the hexagonal wurtzite phase in all samples, but FESEM examination indicated that Er doping resulted in a reduction of dimensions of particles. The assessment of photocatalytic degradation was conducted using Direct Red 31 (DR-31) dye [73]. Among all samples, EZ2 (2.5 at. wt% Er) had the best degrading efficiency at 99.1%. Elevating Er^{3+} concentration above the optimal level led to decreased activity, maybe due to dopant aggregation or excessive defect generation serving as recombination sites.

Jain et al. investigated the photocatalytic properties of Er-doped ZnO nanoparticles produced by a solid-state reaction technique. Doping concentrations between 1 and 5% by weight were examined for the deterioration of Remazol Red Brilliant F3B (RR180) dye. XRD examination revealed a little leftward shift in peak locations with elevated Er content, indicating lattice deformation and suppression of particle development [74]. A continuous reduction in band gap energy was seen with increased Er^{3+} concentrations, enhancing electron excitation under visible light. Optimal photocatalytic performance was observed at 3 wt % Er, with further increases leading to reduced efficiency, possibly owing to light penetration blockage and enhanced charge carrier recombination at elevated dopant concentrations [75].

These findings together demonstrate that Er^{3+} doping in ZnO nanoparticles may markedly improve photocatalytic performance by decreasing particle size,

augmenting surface area, moving absorption into the visible spectrum, and improving charge carrier dynamics. Nonetheless, a crucial threshold of dopant concentration exists, beyond which photocatalytic activity diminishes, underscoring the need for optimizing dopant levels [76].

5.6 Pr-Doped Metal Oxides

Chiou et al. produced praseodymium (Pr^{3+}) doped TiO_2 nanoparticles by the sol–gel process and examined their photocatalytic capabilities. The produced nanoparticles underwent calcination at different temperatures, resulting in a phase change from anatase to rutile. Anatase TiO_2, with a band gap of around 3.2 eV, is recognized for its enhanced photocatalytic efficacy relative to the rutile phase [77]. Pr^{3+} doping in the TiO_2 matrix markedly improved photocatalytic activity by promoting increased photo-generated charge transfer between the valence and conduction bands. UV–Visible absorption spectroscopy showed a wavelength shift in the absorption edge from 350 to 520 nm with increasing Pr content, signifying enhanced visible-light absorption. The largest shift occurred at a doping dose of 0.072 mol % Pr. Beyond this concentration, the absorption edge reverted to shorter wavelengths, indicating a decline in light-harvesting efficiency [78].

The band gap of undoped TiO_2 was determined to be 3.20 eV, but Pr doping demonstrated a progressive decrease in the gap between the bands, ultimately reaching 2.80 eV. This constriction is advantageous for visible light photocatalysis since it facilitates the excitation of electrons. Nevertheless, at Pr^{3+} concentrations beyond the optimal threshold, the duration of charge separation decreased owing to heightened recombination, adversely impacting photocatalytic effectiveness [79].

The photocatalytic activity was assessed using phenol as the target contaminant. Pure TiO_2 attained a degradation efficiency of just 42%. The addition of Pr^{3+} enhanced the degradation rate, reaching a maximum of 94.4% for 0.072 mol % Pr-doped TiO_2. Increasing the dopant percentage to 0.22 mol% led to a little reduction in performance to 91.3%, either owing to the emergence of recombination sites or excess dopant obstructing charge mobility [80].

In summary, Pr^{3+} doping augments the photocatalytic efficacy of TiO_2 by enhancing light absorption into the visible spectrum, reducing the gap between bands, and enhancing charge transport dynamics. Maintaining an adequate dopant concentration is essential to prevent adverse consequences, including diminished charge separation efficiency and spectral blue shifts [81].

5.7 Nd-Doped Metal Oxides

Neodymium (Nd^{3+}) doping has garnered significant interest in enhancing the photocatalytic efficacy of semiconductors of metal oxide owing to its capacity to influence particle size, band gap energy, and charge transport recombination dynamics.

Mzoughi et al. produced neodymium-doped zirconium dioxide (ZrO_2) nanoparticles using the sol–gel technique [82]. X-ray diffraction (XRD) examination verified that the material maintained its tetragonal crystalline form after doping. Scanning electron microscopy (SEM) demonstrated a significant reduction in particle size from 43 nm in pure ZrO_2 to 20 nm in Nd-doped ZrO_2. The photocatalytic efficacy was assessed using methyl orange (MO) dye. Pure ZrO_2 exhibited deterioration mostly in the UV spectrum with an efficiency of 68%, but 9% Nd-doped ZrO_2 showed enhanced activity in the visible spectrum, achieving 99% degradation efficiency after 120 min [43]. This improvement is due to the drop in band gap energy from 2.8 eV (pure) to 2.6 eV (doped), which enhances light absorption and charge carrier dynamics.

Zhang et al. similarly generated Nd-doped ZnO nanoparticles using the sol–gel method. The XRD results validated the wurtzite structure of ZnO. The photocatalytic efficacy was evaluated against Congo Red dye under visual illumination [45]. The findings demonstrated a significant association between Nd doping concentration and photocatalytic efficacy, with 4% Nd-doped ZnO attaining the greatest degradation rate of 93.7% after 30 min of visible light exposure. The performance enhancement is mostly attributable to improved light absorption and effective charge carrier separation resulting from Nd inclusion [83].

Alam et al. synthesized Nd-doped ZnO nanoparticles by the process of precipitation and assessed their photocatalytic efficacy against methylene blue (MB) dye. Neodymium concentrations varying from 3 to 15 wt% were evaluated. Fluorescence spectroscopy revealed a change in the emission band from ultraviolet (367 nm for pure ZnO) to the faint blue range (380–474 nm) after Nd doping. The spectrum alterations signify defect creation and shallow donor levels linked to the dopant, facilitating charge separation and reducing recombination rates [84]. Thus, the photocatalytic activity escalated in direct correlation with the concentration of Nd doping, validating Nd's function in augmenting photo-efficiency via the modulation of recombination and the enhancement of surface-active sites. In conclusion, Nd^{3+} doping in ZrO_2 and ZnO enhances photocatalytic degradation under visible light by cutting the band gap, decreasing particle size, and facilitating improved electron–hole separation. The suitable dopant concentration is essential for enhancing the photocatalytic efficacy of these metallic oxide systems [85].

5.8 Eu-Doped Metal Oxides

The incorporation of rare earth elements like europium (Eu^{3+}) has been investigated to enhance the photocatalytic efficacy of metal oxide semiconductors by altering

their optical, morphological and structural characteristics [86]. Using the technique of precipitation, Kumar et al. produced europium-doped zinc oxide nanoparticles. X-ray diffraction (XRD) investigation verified that both doped and pure ZnO maintained the hexagonal wurtzite structure, indicating no substantial structural change due to doping. Methyl orange (MO) dye photocatalytic degradation experiments conducted under UV light have demonstrated that photocatalytic efficacy rises with increasing Eu content. The improvement was ascribed to the enhanced production of hydroxyl (OH^-) and hydroperoxyl (HO_2^-) radicals, potent oxidants generated by UV irradiation as a result of effective charge carrier formation and separation. Pure ZnO decomposes 75.7% of MO in 180 min, but 1% Eu-doped ZnO achieved 95.3% degradation under the same circumstances [87].

In a similar manner, Korake et al. used a low-temperature microwave-assisted method to create Eu-doped ZnO. The XRD pattern validated the hexagonal wurtzite phase of ZnO. The band gap decreased with the augmentation of Eu concentration, decreasing from 3.34 eV in pure ZnO to 3.00 eV in 0.5% Eu-doped ZnO. Brunauer–Emmett–Teller (BET) surface area studies indicated a rise from 42 m^2/g for pure ZnO to 49m^2/g for 0.2% Eu-doped ZnO, indicating a decrease in nanoparticle size [88]. The photocatalytic degradation of MO under UV light enhanced with increasing Eu concentration, with 0.2 mol % Eu-doped ZnO exhibiting optimum activity 91% degradation of MO in 180 min due to enhanced surface area and charge carrier separation [89]. Bouras et al. [90] examined Eu-doped SnO_2 nanostructures produced by a hydrothermal technique. The research demonstrated that doping with Eu modified the shape of the nanomaterials, shifting from nanorods (pure SnO_2) to nanosheets and then reverting to nanorods at higher doping concentrations. XRD measurements indicated a little rightward shift in diffraction peaks due to doping, implying lattice strain or replacement [90]. Photoluminescence (PL) spectra revealed two discrete emission bands one in the UV area at 350 nm (weak) and another in the visible region at 666 nm (strong), the latter ascribed to oxygen vacancies and electron transfer from SnO_2 to Eu^{3+} ions. Despite the elevated Eu content resulting in enhanced PL intensity, normally signifying an increased recombination rate, the 10 wt% Eu-doped SnO_2 yet demonstrated substantial photocatalytic degradation efficiency of (RhB). This was mostly attributable to the augmented surface area and UV absorbance, which offset the heightened recombination rate [91]. In conclusion, Eu^{3+} doping in ZnO and SnO_2 markedly improves photocatalytic performance under visible or UV light. The enhancements are mostly attributed to decreased band gaps, augmented surface area, defect-induced charge separation, and morphological alterations, all of which facilitate improved formation and usage of reactive oxygen species for dye degradation [92] (Table 4.2; Figs. 4.2 and 4.3).

Table 4.2 Synthesis and degradation methods of various rare earth doped metal oxide nanoparticles

Material	Method	Degradation efficiency%	References
2.5% Er:ZnO	Combustion	99.1	[86]
1% Er:ZnO	Solid state reaction	82	[87]
2% Er:ZnO	Solid state reaction	90	[87]
3% Er:ZnO	Solid state reaction	99	[87]
4% Er:ZnO	Solid state reaction	70	[87]
0.4% Er: CeO_2	Hydrothermal	94	[88]
Pr:TiO_2	Acid-peptized sol–gel	94.4	[77]
Pure ZrO_2	Polymer-assisted	68	[37]
Nd:ZrO_2	Sol–gel	99	[43]
4% Nd:ZnO	Sol–gel	93.7	[43]
1% Eu:ZnO	Precipitation	75.7	[51]
0.2% Eu:ZnO	Microwave-assisted	91	[51]
1% Eu:SnO_2	Hydrothermal	74	[51]
3% Eu:SnO_2	Hydrothermal	70	[51]
5% Eu:SnO_2	Hydrothermal	60	[51]
7% Eu:SnO_2	Hydrothermal	85	[51]
10% Eu:SnO_2	Hydrothermal	90	[51]
2% Eu:Bi2WO_6	Hydrothermal	73.7	[53]
5% Eu:Bi2WO_6	Hydrothermal	96.2	[53]
Eu:$BiVO_4$	Hydrothermal	93.6	[54]
Nd:TiO_2	Hydrothermal	100	[84]
Er:TiO_2	Solvothermal	98.78	[54]
4% Pr:Bi_2O_3	Acrylamide polymerization	70.4	[74]
0.05% Sm:TiO_2	Microwave-assisted sol–gel method	98	[59]
0.1% Sm:TiO_2	Microwave-assisted sol–gel method	96	[59]
0.6%Gd:SnO_2	Sol–gel	100	[60]
3%Gd:ZnO	Sonochemical	92.76%	[73]
1%Gd:$BiFeO_3$	Sol–gel	34.2%	[74]
3%Gd:$BiFeO_3$	Sol–gel	56.8%	[74]
5%Gd:$BiFeO_3$	Sol–gel	42.8%	[74]
0.5% Ce:ZnO	Combustion method	85	[48]
2.5% Ce:ZnO	Combustion method	95	[48]
3.28% Ce:ZnO	Combustion method	100	[48]
3% Ce:ZnO	Hydrothermal	69	[48]
1% Ce:ZnO	Combustion method	51	[52]

(continued)

Table 4.2 (continued)

Material	Method	Degradation efficiency%	References
CeO2-TiO_2	Polymer-assisted method	24	[52]
3% Ce:ZnO	Combustion method	69	[52]
5% Ce:ZnO	Combustion method	64	[52]
1% Sm:TiO_2	Modified-ultrasonic assisted sol–gel	69	[60]
4.8% Er:ZnO	Homogenous precipitation	97.3	[47]
3% Dy:$ZnWO_4$	Hydrothermal	97.46	[73]

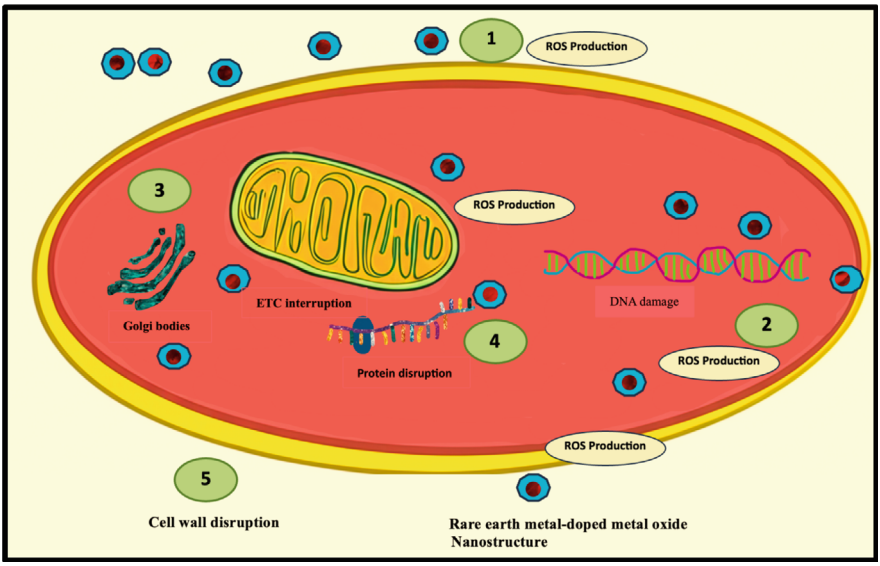

Fig. 4.2 Antibacterial mechanism of rare earth metal-doped nanostructure

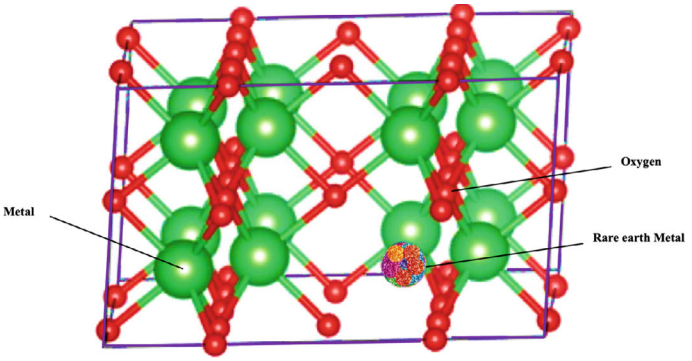

Fig. 4.3 Structure of rare earth metal-doped nanoparticle metal oxide

6 Application of RE-Doped Materials in Wastewater Treatment and Industries

Rare earth (RE)-doped materials are attracting a lot of interest in industrial and wastewater treatment applications because of their distinct optical characteristics, electronic structures, and catalytic capabilities. These substances are excellent choices for eliminating a range of organic and inorganic contaminants from wastewater because of their improved photocatalytic and adsorption capabilities [93]. In photocatalysis, when elements like cerium (Ce), lanthanum (La), europium (Eu), and terbium (Tb) are doped into semiconductors like TiO_2 or ZnO, one of the most promising uses of RE-doped materials is found. Under solar or artificial light irradiation, this doping method enhances visible light absorption, inhibits electron–hole recombination, and boosts photocatalytic performance, making it easier to break down persistent organic pollutants like dyes, phenols, and medications. Indicatively, the Ce-doped TiO_2 has shown superior efficacy in the deterioration of rhodamine B and methylene blue because of its high redox potential and oxygen storage capacity [94]. Furthermore, the elevated surface area and metal ion affinity of RE-doped metal oxides render them suitable candidates for the adsorption-based elimination of heavy metal ions, including chromium, arsenic and lead from industrial effluents. Additionally, RE-doped luminous nanoparticles are used for the real-time identification and monitoring of pollutants, hence facilitating more precise and efficient remediation methods. Advanced oxidation processes (AOPs) in the industrial sectors employ RE-doped catalysts to treat high-strength wastewater from the pharmaceutical, petrochemical, and textile sectors [95]. The lifespan, selectivity, and thermal stability of catalysts may all be improved by adding RE ions to catalytic systems. These developments establish RE-doped materials as essential elements in the shift to treatment of waste water systems that are more sustainable and productive. Recent reviews, like the one published in Environmental Science: Nano by Raliya et al. [96], indicate that the use of RE-doped nanomaterials in wastewater remediation is not only technically possible but also consistent with green chemistry principles, indicating their potential importance in future industrial and environmental applications.

7 Economic Aspects

The expense of adsorbents is a crucial consideration for their practical use. Nevertheless, cost calculations are hardly discussed in the scholarly literature. Most studies emphasize laboratory-scale assessments of adsorption capability, often overlooking economic factors. The market price of zeolites is roughly US$0.03 to US$0.12 per kilogram, Fuller's earth is around US$0.04 per kilogram, and commercial activated carbon is marketed at approximately US$2.00 to US$2.20 per kilogram. However, straight comparisons of adsorbent pricing might be deceptive without assessing their individual features and adsorption efficiency [97].

The term "low-cost adsorbents" often refers only to the raw market price of certain materials. In real situations, the economic feasibility of these materials is often undermined by costly regeneration and treatment procedures. A thorough assessment must take into account several considerations, including local availability, transportation expenses, treatment and modification needs, recyclability, and the overall longevity of the adsorbent [98].

To improve adsorption capacity and selectivity, pre-treatment techniques such as drying, autoclaving, or chemical modification (e.g., cross-linking with organic or inorganic agents) are often used. These therapies may markedly elevate operating expenses. The regeneration process may need considerable energy or solvent consumption, and the proper disposal or handling of depleted adsorbents is a significant and sometimes neglected challenge [99].

Although some adsorbents may seem expensive initially, their long-term reusability and ease of regeneration might make them more cost-effective across their whole existence. Consequently, a life-cycle cost analysis encompassing synthesis, use, regeneration, and disposal is crucial for assessing the actual cost-effectiveness of an adsorbent.

Chitosan, cyclodextrin, and their composites have superior adsorption capabilities. Nonetheless, their extensive use is impeded by substantial starting expenses and intricate synthesis processes. Notwithstanding their promise, there is an absence of comprehensive evaluations of these materials from a whole life-cycle view point [100].

8 Future Prospects

The use of rare earth element (REE)-doped biodegradable polymers in the adsorption and degradation of synthetic dyes offers a viable approach for sustainable wastewater treatment. With the escalation of industrial pollution, especially from textile and dye sectors, the establishment of productive and environment-friendly remediation approaches has become vital. In this context, integrating the unique physicochemical characteristics of rare earth elements with biodegradable polymer matrices is an appealing approach. These hybrid materials have significant adsorption capabilities, remarkable photocatalytic activity, and environmental friendliness, making them suitable for multifunctional water treatment applications [101]. Future research is anticipated to concentrate on the design and synthesis of materials that concurrently provide adsorption, photocatalysis, and antibacterial properties. The integration of rare earth elements, like lanthanum or cerium, into biodegradable polymers has shown an improvement in photocatalytic degradation of colors while maintaining biocompatibility. These multifunctional materials may substantially advance the development of next-generation wastewater treatment systems with improved performance and adaptability [102]. A primary focus of current research is the improvement of photocatalytic efficiency. Doping biodegradable polymers with rare earth elements may provide intermediate band gap energy levels, enhancing the absorption of light

and facilitating efficient charge transport separation, therefore expediting dye degradation rates. Future research may investigate sophisticated doping techniques and the use of innovative polymer matrices to enhance these capabilities further [103]. The implementation of green synthesis techniques for the production of REE-doped biodegradable polymers is expected to increase. Employing plant-derived extracts or bio-waste for nanoparticle synthesis can reduce environmental impact and is consistent with the global focus on sustainable chemical practices. These environmentally sustainable methods are poised to significantly contribute to the advancement of this domain [104]. Research must focus on the scalability, durability, and versatility of these materials for practical applications in water treatment systems. Examinations of their efficacy in intricate and fluctuating wastewater matrices, with their enduring environmental consequences, will be crucial. Furthermore, the issues associated with the restricted supply and elevated costs of rare earth elements must be recognized. To address these issues, further research might concentrate on identifying alternative, earth-abundant dopants with similar effectiveness, as well as on devising efficient rare earth element recovery and recycling methods from used materials [105]. In conclusion, REE-doped biodegradable polymers provide significant promise for enhancing sustainable wastewater treatment. Achieving this potential requires multidisciplinary cooperation, advancements in materials science, and the use of green chemistry concepts to address current limits and enhance practical applications in environmental restoration [106].

9 Conclusion

Rare earth doping has become a flexible and efficient method for band gap technology in transition metal oxides, facilitating improved photocatalytic performance. This paper examines critical elements of materials development and doping stability related to rare earth-doped oxides of metals. The integration of rare earth elements into metal oxide matrices causes a red shift in the absorption spectra, broadening light absorption into the visible range, an essential aspect for solar-driven applications. Moreover, methodologies for synthesizing materials characterized by high crystallinity and extensive specific surface areas, as assessed by BET analysis, are comprehensively examined. The photocatalytic efficiency of metal oxides is markedly enhanced by rare earth doping, either by band gap reduction or diminishing charge carrier reshuffling. Doping with suitable rare earth ions significantly improves the separation of photo-generated electron–hole pairs, successfully preventing their recombination and enhancing photocatalytic effectiveness. These doped systems frequently exhibit an apparent reduction in the optical band gap energy, improving light consumption. A detailed description of the photocatalytic performance of several rare earth-doped metallic oxides is presented in table format for comparative analysis. Although the majority of investigations so far have focused on dye degradation as a case study reaction, the potential use of these materials for photocatalytic hydrogen (H_2) production remains underexplored. Not with-standing their

advantageous band alignments and beneficial charge transfer properties essential for effective photocatalytic water splitting, these materials have not been extensively used in this application. In conclusion, even though the development of rare earth-doped metal oxide photocatalysts has advanced significantly, there is still a great deal of untapped potential in this field. A significant difficulty that persists is the standardization of photocatalytic efficiency measurements to provide valid comparisons and assess economic viability for practical implementation. This analysis provides a framework for further investigations focused on maximizing the potential of rare earth-doped nanomaterials for photochemical hydrogen production.

References

1. Lonngren, K.E., Bai, E.W.: On the global warming problem due to carbon dioxide. Energy Policy **36**(4), 1567–1568 (2008)
2. Mehtab, A., Ahmed, J., Alshehri, S.M., Mao, Y., Ahmad, T.: Rare earth doped metal oxide nanoparticles for photocatalysis: a perspective. Nanotechnology **33**(14), 142001 (2022)
3. Heard, B.P., Brook, B.W., Wigley, T.M., Bradshaw, C.J.: Burden of proof: a comprehensive review of the feasibility of 100% renewable-electricity systems. Renew. Sustain. Energy Rev. **76**, 1122–1133 (2017)
4. Brown, V.M., Jordan, D.H.M., Tiller, B.A.: The effect of temperature on the acute toxicity of phenol to rainbow trout in hard water. Water Res. **1**(8–9), 587–594 (1967)
5. Bak, T., Nowotny, J., Rekas, M., Sorrell, C.C.: Photo-electrochemical hydrogen generation from water using solar energy. Materials-related aspects. Int. J. Hydrogen Energy **27**(10), 991–1022 (2002)
6. Deng, Y., Yeo, B.S.: Characterization of electrocatalytic water splitting and CO_2 reduction reactions using in situ/operando Raman spectroscopy. ACS Catal. **7**(11), 7873–7889 (2017)
7. Esposito, D.V., Chen, J.G., Birkmire, R.W., Chang, Y., Gaillard, N.: Hydrogen production from photo-driven electrolysis of biomass-derived oxygenates: a case study on methanol using Pt-modified WO3 thin film electrodes. Int. J. Hydrogen Energy **36**(16), 9632–9644 (2011)
8. Jose, V.: Photobiological hydrogen as a renewable fuel. Holistic Appr. Environ. **11**(2), 67–71 (2021)
9. Ghirardi, M.L., Dubini, A., Yu, J., Maness, P.C.: Photobiological hydrogen-producing systems. Chem. Soc. Rev. **38**(1), 52–61 (2009)
10. Baykara, S.Z.: Experimental solar water thermolysis. Int. J. Hydrogen Energy **29**(14), 1459–1469 (2004)
11. Helseth, L.E.: Electrical energy harvesting from water droplets passing a hydrophobic polymer with a metal film on its back side. J. Electrostat. **81**, 64–70 (2016)
12. Yılmaz, S., Selim, H.: A review on the methods for biomass to energy conversion systems design. Renew. Sustain. Energy Rev. **25**, 420–430 (2013)
13. Saidur, R., Abdelaziz, E.A., Demirbas, A., Hossain, M.S., Mekhilef, S.: A review on biomass as a fuel for boilers. Renew. Sustain. Energy Rev. **15**(5), 2262–2289 (2011)
14. Ahmad, T., Farooq, U., Phul, R.: Fabrication and photocatalytic applications of perovskite materials with special emphasis on alkali-metal-based niobates and tantalates. Ind. Eng. Chem. Res. **57**(1), 18–41 (2018)
15. Ikram, S., Ashraf, F., Alzaid, M., Mahmood, K., Amin, N., Haider, S.A.: Role of nature of rare earth ion dopants on structural, spectral, and magnetic properties in spinel ferrites. J. Supercond. Novel Magn. **34**, 1745–1751 (2021)
16. Tentu, R.D., Basu, S.: Photocatalytic water splitting for hydrogen production. Curr. Opin. Electrochem. **5**(1), 56–62 (2017)

17. Luan, J., Li, Y.: Photocatalytic water splitting for hydrogen production with Gd2MSbO7 (M= Fe, In, Y) photocatalysts under visible light irradiation. Materials **8**(1), 16–30 (2014)
18. Miseki, Y., Sayama, K.: Photocatalytic water splitting for Solar hydrogen production using the carbonate effect and the Z-scheme reaction. Adv. Energy Mater. **9**(23), 1801294 (2019)
19. Singh, A.K., Mathew, K., Zhuang, H.L., Hennig, R.G.: Computational screening of 2D materials for photocatalysis. J. Phys. Chem. Lett. **6**(6), 1087–1098 (2015)
20. Raizada, P., Soni, V., Kumar, A., Singh, P., Khan, A.A.P., Asiri, A.M., Thakur, V.K., Nguyen, V.H.: Surface defect engineering of metal oxides photocatalyst for energy application and water treatment. J. Materiomics **7**(2), 388–418 (2021)
21. Naldoni, A., Allieta, M., Santangelo, S., Marelli, M., Fabbri, F., Cappelli, S., Bianchi, C.L., Psaro, R., Dal Santo, V.: Effect of nature and location of defects on bandgap narrowing in black TiO_2 nanoparticles. J. Am. Chem. Soc. **134**(18), 7600–7603 (2012)
22. Prévot, M.S., Sivula, K.: Photoelectrochemical tandem cells for solar water splitting. J. Phys. Chem. C **117**(35), 17879–17893 (2013)
23. Navarro, R.M., Sanchez-Sanchez, M.C., Alvarez-Galvan, M.C., Del Valle, F., Fierro, J.L.G.: Hydrogen production from renewable sources: biomass and photocatalytic opportunities. Energy Environ. Sci. **2**(1), 35–54 (2009)
24. Li, P., Tian, Y., Du, M., Xie, Q., Chen, Y., Ma, L., Huang, Y., Yin, Z., Xu, H., Wu, X.: Mechanism of rotenone toxicity against *Plutella xylostella*: new perspective from a spatial metabolomics and lipidomics study. J. Agric. Food Chem. **71**(1), 211–222 (2022)
25. Ali, M., Sreekrishnan, T.R.: Aquatic toxicity from pulp and paper mill effluents: a review. Adv. Environ. Res. **5**(2), 175–196 (2001)
26. Klavarioti, M., Mantzavinos, D., Kassinos, D.: Removal of residual pharmaceuticals from aqueous systems by advanced oxidation processes. Environ. Int. **35**(2), 402–417 (2009)
27. Robinson, T., McMullan, G., Marchant, R., Nigam, P.: Remediation of dyes in textile effluent: a critical review on current treatment technologies with a proposed alternative. Biores. Technol. **77**(3), 247–255 (2001)
28. Ogugbue, C.J., Sawidis, T.: Bioremediation and detoxification of synthetic wastewater containing triarylmethane dyes by *Aeromonas hydrophila* isolated from industrial effluent. Biotechnol. Res. Int. **2011**(1), 967925 (2011)
29. Liu, D., Huang, J., Tao, X., Wang, D.: One-step synthesis of C-Bi_2WO_6 crystallites with improved photo-catalytic activities under visible light irradiation. RSC Adv. **5**(81), 66464–66470 (2015)
30. Barrera, A., Tzompantzi, F., Campa-Molina, J., Casillas, J.E., Pérez-Hernández, R., Ulloa-Godinez, S., Velásquez, C., Arenas-Alatorre, J.: Photocatalytic activity of Ag/Al_2O_3–Gd_2O_3 photocatalysts prepared by the sol–gel method in the degradation of 4-chlorophenol. RSC Adv. **8**(6), 3108–3119 (2018)
31. Brites, F.F., Santana, V.S., Fernandes-Machado, N.R.C.: Effect of support on the photocatalytic degradation of textile effluents using Nb_2O_5 and ZnO: photocatalytic degradation of textile dye. Top. Catal. **54**, 264–269 (2011)
32. Li, H., Wang, G., Zhang, F., Cai, Y., Wang, Y., Djerdj, I.: Surfactant-assisted synthesis of CeO_2 nanoparticles and their application in wastewater treatment. RSC Adv. **2**(32), 12413–12423 (2012)
33. Farooq, U., Chaudhary, P., Ingole, P.P., Kalam, A., Ahmad, T.: Development of cuboidal $KNbO_3$@ α-Fe_2O_3 hybrid nanostructures for improved photocatalytic and photoelectrocatalytic applications. ACS Omega **5**(32), 20491–20505 (2020)
34. Akhoondi, A., Ghaebi, H., Karuppasamy, L., Rahman, M.M., Sathishkumar, P.: Recent advances in hydrogen production using MXenes-based metal sulfide photocatalysts. Synthesis and Sintering **2**(1), 37–54 (2022)
35. Ran, J., Zhang, J., Yu, J., Jaroniec, M., Qiao, S.Z.: Earth-abundant cocatalysts for semiconductor-based photocatalytic water splitting. Chem. Soc. Rev. **43**(22), 7787–7812 (2014)
36. Khan, M.M., Adil, S.F., Al-Mayouf, A.: Metal oxides as photocatalysts. J. Saudi Chem. Soc. **19**(5), 462–464 (2015)

37. Yan, Y., Xia, B. Y., Ge, X., Liu, Z., Fisher, A., Wang, X.: A flexible electrode based on iron phosphide nanotubes for overall water splitting. Chem. A Eur. J. **21**(50), 18062–18067 (2015)
38. Ju, L., Dai, Y., Wei, W., Li, M., Liang, Y., Huang, B.: One-dimensional cadmium sulphide nanotubes for photocatalytic water splitting. Phys. Chem. Chem. Phys. **20**(3), 1904–1913 (2018)
39. Iwashina, K., Iwase, A., Ng, Y.H., Amal, R., Kudo, A.: Z-schematic water splitting into H_2 and O_2 using metal sulfide as a hydrogen-evolving photocatalyst and reduced graphene oxide as a solid-state electron mediator. J. Am. Chem. Soc. **137**(2), 604–607 (2015)
40. Paramasivam, I., Jha, H., Liu, N., Schmuki, P.: A review of photocatalysis using self-organized TiO_2 nanotubes and other ordered oxide nanostructures. Small **8**(20), 3073–3103 (2012)
41. Mangrulkar, P.A., Joshi, M.M., Tijare, S.N., Polshettiwar, V., Labhsetwar, N.K., Rayalu, S.S.: Nano cobalt oxides for photocatalytic hydrogen production. Int. J. Hydrogen Energy **37**(13), 10462–10466 (2012)
42. Kalam, A., Al-Sehemi, A.G., Ashrafuzzaman, M., Allami, S.A.S., Sharif, A.M., Yadav, P., Assiri, M.A., Du, G.: Synthesis of gadolinium doped ZnO nanomaterials using the modified-solvothermal method and studied the effect of gadolinium on the structural, morphological, and optical properties. J. Inorgan. Organometallic Polymers Mater. **33**(10), 3076–3086 (2023)
43. Selvaraj, S., Mohan, M.K., Navaneethan, M., Ponnusamy, S., Muthamizhchelvan, C.: Synthesis and photocatalytic activity of Gd doped ZnO nanoparticles for enhanced degradation of methylene blue under visible light. Mater. Sci. Semicond. Process. **103**, 104622 (2019)
44. Danish, M.S.S., Estrella, L.L., Alemaida, I.M.A., Lisin, A., Moiseev, N., Ahmadi, M., Nazari, M., Wali, M., Zaheb, H., Senjyu, T.: Photocatalytic applications of metal oxides for sustainable environmental remediation. Metals **11**(1), 80 (2021)
45. Zhang, X., Zhou, G., Zhang, H., Wu, C., Song, H.: Characterization and activity of visible light–driven TiO_2 photocatalysts co-doped with nitrogen and lanthanum. Transition Met. Chem. **36**, 217–222 (2011)
46. Medhi, R., Marquez, M.D., Lee, T.R.: Visible-light-active doped metal oxide nanoparticles: review of their synthesis, properties, and applications. ACS Appl. Nano Mater. **3**(7), 6156–6185 (2020)
47. Chen, H., Wang, L.: Nanostructure sensitization of transition metal oxides for visible-light photocatalysis. Beilstein J. Nanotechnol. **5**(1), 696–710 (2014)
48. Yu, J., Yu, J.C., Cheng, B., Zhao, X.: Photocatalytic activity and characterization of the sol-gel derived Pb-doped TiO_2 thin films. J. Sol-Gel Sci. Technol. **24**, 39–48 (2002)
49. Natarajan, T.S., Natarajan, K., Bajaj, H.C., Tayade, R.J.: Enhanced photocatalytic activity of bismuth-doped TiO_2 nanotubes under direct sunlight irradiation for degradation of Rhodamine B dye. J. Nanopart. Res. **15**(5), 1–18 (2013)
50. Kumaresan, L., Mahalakshmi, M., Palanichamy, M., Murugesan, V.: Synthesis, characterization, and photocatalytic activity of Sr^{2+} doped TiO_2 nanoplates. Ind. Eng. Chem. Res. **49**(4), 1480–1485 (2010)
51. Kim, S.P., Choi, M.Y., Choi, H.C.: Photocatalytic activity of SnO_2 nanoparticles in methylene blue degradation. Mater. Res. Bull. **74**, 85–89 (2016)
52. Mora, J.R., Flores-Carrasco, G., Juárez, H., Pacio, M., Olvera, M.D.L.L., Rabanal, M.E.: Ce-doped ZnO nanonails synthesized by a simple thermal evaporation method for photocatalytic degradation. Opt. Mater. **157**, 116156 (2024)
53. Meshram, S.P., Adhyapak, P.V., Pardeshi, S.K., Mulla, I.S., Amalnerkar, D.P.: Sonochemically generated cerium doped ZnO nanorods for highly efficient photocatalytic dye degradation. Powder Technol. **318**, 120–127 (2017)
54. Lone, I.H., Kalam, A., Ahmed, J., Alhokbany, N., Alshehri, S.M., Ahmad, T.: Quenching assisted reverse micellar synthesis and electrical properties of high surface area BiFeO3 nanoparticles. J. Nanosci. Nanotechnol. **20**(6), 3823–3831 (2020)
55. Li, F.B., Li, X.Z., Hou, M.F., Cheah, K.W., Choy, W.C.H.: Enhanced photocatalytic activity of $Ce3^{+}$-TiO_2 for 2-mercaptobenzothiazole degradation in aqueous suspension for odour control. Appl. Catal. A **285**(1–2), 181–189 (2005)

56. Saqib, N.U., Adnan, R., Shah, I.: A mini-review on rare earth metal-doped TiO_2 for photocatalytic remediation of wastewater. Environ. Sci. Pollut. Res. **23**, 15941–15951 (2016)
57. Kuzhalosai, V., Subash, B., Shanthi, M.: A novel sunshine active cerium loaded zinc oxide photocatalyst for the effective degradation of AR 27 dye. Mater. Sci. Semicond. Process. **27**, 924–933 (2014)
58. Milanova, M., Tsvetkov, M.: Rare earths doped materials. Crystals **11**(3), 231 (2021)
59. Wang, C., Zeng, T., Zhu, S., Gu, C.: Synergistic mechanism of rare-earth modification TiO_2 and photodegradation on benzohydroxamic acid. Appl. Sci. **9**(2), 339 (2019)
60. Arasi, S.E., Madhavan, J., Antony Raj, M.V.: Effect of samarium (Sm3+) doping on structural, optical properties and photocatalytic activity of titanium dioxide nanoparticles. J. Taibah Univ. Sci. **12**(2), 186–190 (2018)
61. Benammar, I., Salhi, R., Deschanvres, J.L., Maalej, R.: The effect of rare earth element (Er, Yb) doping and heat treatment on suspension stability of Y_2O_3 nanoparticles elaborated by sol-gel method. J. Market. Res. **9**(6), 12634–12642 (2020)
62. Xia, W., Pei, Z., Leng, K., Zhu, X.: Research progress in rare earth-doped perovskite manganite oxide nanostructures. Nanoscale Res. Lett. **15**(9), 1–55 (2020)
63. Faraz, M., Naqvi, F.K., Shakir, M., Khare, N.: Synthesis of samarium-doped zinc oxide nanoparticles with improved photocatalytic performance and recyclability under visible light irradiation. New J. Chem. **42**(3), 2295–2305 (2018)
64. Depner, S.W., Kort, K.R., Banerjee, S.: Precursor control of crystal structure and stoichiometry in twin metal oxide nanocrystals. Cryst. Eng. Comm. **11**(5), 841–846 (2009)
65. Vaidya, S., Ahmad, T., Agarwal, S., Ganguli, A.K.: Nanocrystalline oxalate/carbonate precursors of Ce and Zr and their decompositions to CeO_2 and ZrO_2 nanoparticles. J. Am. Ceram. Soc. **90**(3), 863–869 (2007)
66. Ahmad, T., Ganguli, A.K.: Structural and dielectric characterization of nanocrystalline (Ba, Pb) ZrO_3 developed by reverse micellar synthesis. J. Am. Ceram. Soc. **89**(10), 3140–3146 (2006)
67. Farooq, U., Ahmed, J., Alshehri, S.M., Ahmad, T.: High-surface-area sodium tantalate nanoparticles with enhanced photocatalytic and electrical properties prepared through polymeric citrate precursor route. ACS Omega **4**(21), 19408–19419 (2019)
68. Farooq, U., Phul, R., Alshehri, S.M., Ahmed, J., Ahmad, T.: Electrocatalytic and enhanced photocatalytic applications of sodium niobate nanoparticles developed by citrate precursor route. Sci. Rep. **9**(1), 4488 (2019)
69. Phuruangrat, A., Thipkonglas, S., Thongtem, T., Thongtem, S.: Hydrothermal synthesis and characterization of Dy-doped MoO_3 nanobelts for using as a visible-light-driven photocatalyst. Mater. Lett. **195**, 37–40 (2017)
70. Phul, R., Khan, M.M., Sardar, M., Ahmed, J., Ahmad, T.: Multifunctional electrochemical properties of synthesized non-precious iron oxide nanostructures. Crystals **10**(9), 1–14 (2020)
71. Ahmad, T., Khatoon, S., Coolahan, K., Lofland, S.E.: Solvothermal synthesis, optical and magnetic properties of nanocrystalline Cd1− xMnxO (0.04< x= 0.10) solid solutions. J. Alloy. Compd. **558**, 117–124 (2013)
72. Phul, R., Perwez, M., Ahmed, J., Sardar, M., Alshehri, S., Alhokbany, N., Majeed Khan. M.A., Ahmad, T.: Efficient multifunctional catalytic and sensing properties of synthesized ruthenium oxide nanoparticles. Catalysts **10**(7), 1–12 (2020)
73. Senol, S.D.: Hydrothermal derived nanostructure rare earth (Er, Yb)-doped ZnO: structural, optical and electrical properties. J. Mater. Sci. Mater. Electron. **27**, 7767–7775 (2016)
74. Ahmad, T., Phul, R.: Magnetic iron oxide nanoparticles as contrast agents: hydrothermal synthesis, characterization and properties. Solid State Phenom. **232**, 111–145 (2015)
75. Jain, S.K., Farooq, U., Jamal, F., Kalam, A., Ahmad, T.: Hydrothermal assisted synthesis and structural characterization of Zn doped SnO_2 nanoparticles for catalytic reduction of 4-nitrophenol. Mater. Today Proc. **36**, 717–723 (2021)
76. Zhou, Y.: Controllable design, synthesis and characterization of nanostructured rare earth metal oxides. Phys. Sci. Rev. **5**(3), 20180084 (2020)

77. Chiou, C.H., Juang, R.S.: Photocatalytic degradation of phenol in aqueous solutions by Pr-doped TiO_2 nanoparticles. J. Hazard. Mater. **149**(1), 1–7 (2007)
78. Nasi, R., Esposito, S., Freyria, F.S., Armandi, M., Gadhi, T.A., Hernandez, S., Rivolo, P., Ditaranto, N., Bonelli, B.: Application of reverse micelle sol–gel synthesis for bulk doping and heteroatoms surface enrichment in mo-doped TiO_2 nanoparticles. Materials **12**(6), 937 (2019)
79. Lang, J., Han, Q., Yang, J., Li, C., Li, X., Yang, L., Zhang, Y., Gao, M., Wang, D., Cao, J.: Fabrication and optical properties of Ce-doped ZnO nanorods. J. Appl. Phys. **107**(7) (2010)
80. Ahmad, T., Shahazad, M., Phul, R.: Hydrothermal synthesis, characterization and dielectric properties of zirconia nanoparticles. Mater. Sci. Eng. Int. J **1**(3), 100–104 (2017)
81. Mu, W., Xie, X., Li, X., Zhang, R., Yu, Q., Lv, K., Wei, H., Jian, Y.: Characterizations of Nb-doped WO_3 nanomaterials and their enhanced photocatalytic performance. RSC Adv. **4**(68), 36064–36070 (2014)
82. Mzoughi, M., Anku, W.W., Oppong, S.O., Shukla, S.K., Agorku, E.S., Govender, P.P.: Neodymium doped ZrO_2-graphene oxide nanocomposites: a promising photocatalyst for photodegradation of Eosin Y dye. Adv. Mater. Lett. **7**(12), 946–950 (2016)
83. Murugadoss, G., Jayavel, R., Kumar, M.R.: Structural and optical properties of highly crystalline Ce, Eu and co-doped ZnO nanorods. Superlattices Microstruct. **82**, 538–550 (2015)
84. Alam, U., Khan, A., Ali, D., Bahnemann, D., Muneer, M.: Comparative photocatalytic activity of sol–gel derived rare earth metal (La, Nd, Sm and Dy)-doped ZnO photocatalysts for degradation of dyes. RSC Adv. **8**(31), 17582–17594 (2018)
85. Khade, G.V., Suwarnkar, M.B., Gavade, N.L., Garadkar, K.M.: Sol–gel microwave assisted synthesis of Sm-doped TiO_2 nanoparticles and their photocatalytic activity for the degradation of methyl orange under sunlight. J. Mater. Sci. Mater. Electron. **27**, 6425–6432 (2016)
86. Choudhury, B., Borah, B., Choudhury, A.: Extending photocatalytic activity of TiO_2 nanoparticles to visible region of illumination by doping of cerium. Photochem. Photobiol. **88**(2), 257–264 (2012)
87. Kumar, M., Singh, G., Chauhan, M.S.: Europium (Eu3+)-doped ZnO nanostructures: Synthesis, characterization, and photocatalytic, chemical sensing and preliminary assessment of magnetic properties. Ceram. Int. **47**(12), 17023–17033 (2021)
88. Korake, P.V., Kadam, A.N., Garadkar, K.M.: Photocatalytic activity of Eu3+-doped ZnO nanorods synthesized via microwave assisted technique. J. Rare Earths **32**(4), 306–313 (2014)
89. Bhatia, S., Verma, N.: Photocatalytic activity of ZnO nanoparticles with optimization of defects. Mater. Res. Bull. **95**, 468–476 (2017)
90. Bouras, K.: Re-doped SnO_2 oxides for efficient UV-Vis to infrared photon conversion: application to solar cells. Doctoral dissertation, Université de Strasbourg) (2016)
91. Ahmed, J., Mao, Y.: Ultrafine iridium oxide nanorods synthesized by molten salt method toward electrocatalytic oxygen and hydrogen evolution reactions. Electrochim. Acta **212**, 686–693 (2016)
92. Yuan, J., Choo, E.S.G., Tang, X., Sheng, Y., Ding, J., Xue, J.: Synthesis of ZnO–Pt nanoflowers and their photocatalytic applications. Nanotechnology **21**(18), 185606 (2010)
93. Basseem, M., Emam, A.A., Kamal, F.H., Gamal, A.M., Abo Faraha, S.A.: Novel functionalized of ZnO with Sm^{3+}, La^{3+}, and Sr^{2+}/ZnO single and tri-doped nanomaterials for photocatalytic degradation: synthesis, DFT, kinetics. J. Mater. Sci. **58**(33), 13346–13372 (2023)
94. Shahid, T., Mirza, M., Kosar, S., Ramzan, A., Ismail, A., Fareed, R., Husain, S., Mustafa, S., Yasmeen, N., Ameer, A., Nawaz, A., Safdar, M.: A facile synthesis of metal vanadate incorporated with metal oxide/rare earth metal oxide composite for photocatalytic application. Next Mater. **4**, 100191 (2024)
95. Dhanda, E., Nain, A., Dahiya, S.: A highly effective PANI@(Ce-Er) dual doped ZnO (PCEZ) nanocomposite as UV-light driven photocatalyst for degradation of MB dye: synthesis and characterization. Phys. Scr. **99**(8), 085043 (2024)
96. Raliya, R., Saharan, V., Dimkpa, C., Biswas, P.: Nanofertilizer for precision and sustainable agriculture: current state and future perspectives. J. Agric. Food Chem. **66**(26), 6487–6503 (2017)

97. Akhter, F., Ahmed, J., Pinjaro, M.A., Shaikh, F.A., Arain, H.J., Ahsan, M.J.: Metal-doped carbon dots (MCDs) as efficient nano-adsorbents for detection, monitoring, and degradation of wastewater pollutants: recent progress, challenges, and future prospects. Water Air Soil Pollut. **234**(11), 672 (2023)
98. Ayman, I., Aadil, M., Shahid, M., Khalid, A., Samama, H., Somaily, H.H., Warsi, M.F., Mohamed, R.M.: Wet synthesis of magnetically retrievable Mn/Nd co-doped cobalt ferrites for visible light-driven photocatalytic annihilation of azo dye. Mater. Sci. Semiconductor Process. **178**, 108462 (2024)
99. Hossain, M.K., Hossain, S., Ahmed, M.H., Khan, M.I., Haque, N., Raihan, G.A.: A review on optical applications, prospects, and challenges of rare-earth oxides. ACS Appl. Electron. Mater. **3**(9), 3715–3746 (2021)
100. Kumari, S., Sharma, R., Thakur, N., Kumari, A.: Removal of organic and inorganic effluents from wastewater by using degradation and adsorption properties of transition metal-doped nickel ferrite. Environ. Sci. Pollut. Res. **31**(34), 46526–46545 (2024)
101. Patil, A.S., Patil, A.V., Dighavkar, C.G., Adole, V.A., Tupe, U.J.: Synthesis techniques and applications of rare earth metal oxides semiconductors: a review. Chem. Phys. Lett. **796**, 139555 (2022)
102. Chen, W., Ball, A.S., Cole, I., Yin, H.: Metal-doped carbon dots as fenton-like catalysts and their applications in pollutant degradation and sensing. Sustainability **17**(8), 3642 (2025)
103. Uysal, E., Dursun, H.N., Uysal, E.C., Gürmen, S.: Synthesis of low pH stable, highly photocatalytic alginate hydrogels for methylene blue removal from wastewater. Turk. J. Chem. **49**(2), 154–175 (2025)
104. Hossain, M.K., Raihan, G.A., Akbar, M.A., Kabir Rubel, M.H., Ahmed, M.H., Khan, M.I., Hossain, S., Sen, S.K., Ebne Jalal, M.I., El-Denglawey, A.: Current applications and future potential of rare earth oxides in sustainable nuclear, radiation, and energy devices: a review. ACS Appl. Electron. Mater. **4**(7), 3327–3353 (2022)
105. Subramanian, Y., Le Minh, T., Bahruji, H., Sarifuddin, W.S., Mahadi, A.H., Gubendiran, R.K.,.Muhammed Ali, S.A., Raj, V., Yassin, H., Irvine, J.T.S., Azad, A.K.: Heteroanionic synthesis of lanthanum/neodymium-based titanium oxycarbide: a novel approach with multiple objectives for clean energy and pollutant-free environment. Clean Energy **9**(1), 89–107 (2025)
106. Ahmad, T., Phul, R., Khatoon, N., Sardar, M.: Antibacterial efficacy of Ocimum sanctum leaf extract-treated iron oxide nanoparticles. New J. Chem. **41**(5), 2055–2061 (2017)